

## Two-Fluid Formulation of Lower-Hybrid Drift Instabilities in Current-Sheet Equilibrium with a Guide Field

W. Zhang<sup>1,\*</sup>, Z. Lin<sup>1</sup>, P. H. Yoon<sup>2</sup> and X. Wang<sup>3</sup>

<sup>1</sup> *Department of Physics and Astronomy, UC Irvine, Irvine, CA 92697, USA.*

<sup>2</sup> *Institute for Physical Science and Technology, University of Maryland, College Park, MD 20742-2431, USA.*

<sup>3</sup> *Department of Physics, Auburn University, Alabama 36849, USA.*

Received 30 November 2007; Accepted (in revised version) 6 March 2008

Available online 21 April 2008

---

**Abstract.** A nonlocal two-fluid formulation has been constructed for describing lower-hybrid drift instabilities in current-sheet configuration with a finite guide magnetic field in the context of magnetic reconnection. As a benchmark and verification, a class of unstable modes with multiple eigenstates are found by numerical solutions with guide field turned off. It is found that the most unstable modes are the electrostatic, short-wavelength perturbations in the lower-hybrid frequency range, with wave functions localized at the edge of the current sheet where the density gradient reaches its maximum. It is also found that there exist electrostatic modes located near the center of the current sheet where the current density is maximum. These modes are low-frequency, long-wavelength perturbations. Attempts will be made to compare the current results with those from kinetic theory in the near future since the validity of the fluid theory ultimately needs to be checked with the more fundamental kinetic theory.

**PACS:** 52.35.Vd, 94.30.cp, 52.35.Kt

**Key words:** Lower-hybrid drift instability, guide field, two-fluid model, Harris equilibrium.

---

## 1 Introduction

Lower-hybrid drift instability (LHDI) is of interest mainly due to its possible connection to anomalous resistivity, which is believed to be a possible mechanism to increase the magnetic reconnection rate. Magnetic reconnection [1–3] is one of the most challenging problems in the field of space, astrophysical and laboratory plasmas. Magnetic reconnection plays an essential role in determining the evolution of magnetic topology

---

\*Corresponding author. *Email addresses:* wenluz@uci.edu (W. Zhang), zhihongl@uci.edu (Z. Lin), yoonp@ipst.umd.edu (P. H. Yoon), xywang@physics.auburn.edu (X. Wang)

in relaxation processes, usually accompanied by an observed rapid release of magnetic energy, in these highly conducting plasmas. However, the current simulation and theoretical results based on the Sweet-Parker model addressing the reconnection process predict a much slower reconnection rate than observed due to the extremely small resistivity. This makes it inevitable for the magnetic field to dissipate only in a very narrow sheet, which obstructs the mass outflow and as a consequence, limit the reconnection rate. Although the subsequent Petschek model [4] based on slow shocks allows large mass flows by opening up the outflow channel and thus results in the faster reconnection rates, it was shown later [5, 6] that the Petschek solution is not compatible with smooth resistivity profiles. On the other hand, microinstabilities may enhance resistivity in the reconnection region, where plenty of free energy exists in form of a large relative drift between ions and electrons and large inhomogeneities in pressure. As a result, this anomalous resistivity will increase the reconnection rate. LHDI is one candidate addressing the mechanisms responsible for such an anomalous resistivity. In fact, MRX experiments [7] reported a positive correlation between the lower-hybrid fluctuations and enhanced rates of magnetic reconnection in the center of a reconnecting current sheet.

LHDI is driven by inhomogeneous density, magnetic field, and/or temperature, with maximum growth believed to occur along directions orthogonal to both the magnetic field vector and the direction of the inhomogeneity, which is frequently assumed to be perpendicular to the direction of the magnetic field. The underlying microinstabilities have been considered to be predominantly electrostatic due to their effectiveness in wave-particle interactions.

LHDI without guide field [8–13, 15–18] has been extensively investigated by previous works. Specifically, Batchelor [8] and Davidson [9] formulated the nonlocal theory on LHDI in cylindrical plasma. LHDI type instabilities, for example, velocity-shear driven, Kelvin-Helmholtz-type instabilities, have been studied by Ganguli with his colleagues [10–12], and Gladd *et al.* [13]. The nonlocal theory on the LHDI in Harris equilibrium has been investigated by Huba *et al.* [17] and Yoon [18]. However, in the space and laboratory plasmas, a sheared magnetic field is usually accompanied by a guide magnetic field, which will significantly affect the evolution of instability and may also give rise to some new instabilities that could significantly impact the physics of magnetic reconnection. An implicit, fully kinetic approach by Daughton [21] and a gyrokinetic electron/full kinetic ion model by Lin have been developed to study the lower hybrid drift-instability with a guide field.

In the present paper we report an improved formulation of the nonlocal characteristics of LHDI in an equilibrium geometry with a finite guide field using an electrostatic two-fluid model. A wave function for the LHDI has been derived, which has been numerically solved for a set of parameters. This work is the first result of a series of analytical and numerical works on LHDI and magnetic reconnection, which will eventually lead to the kinetic simulations of fast reconnections with a finite guide field. Comparisons with kinetic theory will be made in the near future in order to verificate the validation of fluid and kinetic theory.

## 2 Nonlocal electrostatic two-fluid theory of LHDI in Harris equilibrium

The present work is based on a electrostatic two-fluid model with an uniform temperature distribution for fully ionized electron-ion plasma. The relevant equations are continuity, momentum, and the Poisson equations,

$$\partial_t n_s + \nabla \cdot (n_s \mathbf{v}_s) = 0, \quad (2.1)$$

$$m_s n_s (\partial_t + \mathbf{v}_s \cdot \nabla) \mathbf{v}_s = q_s n_s (\mathbf{E} + \mathbf{v}_s \times \mathbf{B}) - K T_s \nabla n_s, \quad (2.2)$$

$$\epsilon \nabla \cdot \mathbf{E} = \sum_s q_s n_s, \quad (2.3)$$

$$\mathbf{E} = -\nabla \phi, \quad (2.4)$$

where subscript  $s = he, hi, be, bi$  stands for the Harris electrons and ions, and uniform background electrons and ions, respectively.

In the current formalism, we assume that equilibrium electric field is absent ( $\bar{\mathbf{E}} = 0$ ), and that densities, sheared magnetic field, and the equilibrium flow are inhomogeneous in the  $z$  direction, which at the lowest order satisfy the steady-state equations governing the equilibrium

$$\nabla \cdot (\bar{n}_s \bar{\mathbf{v}}_s) = 0, \quad (2.5)$$

$$m_s \bar{n}_s \bar{\mathbf{v}}_s \cdot \nabla \bar{\mathbf{v}}_s = q_s \bar{n}_s \bar{\mathbf{v}}_s \times \bar{\mathbf{B}} - K T_s \nabla \bar{n}_s, \quad (2.6)$$

$$\sum_s q_s \bar{n}_s = 0. \quad (2.7)$$

The force-balance equation (2.6) and the neutrality equation (2.7) hold

$$(\nabla \times \bar{\mathbf{B}}) \times \bar{\mathbf{B}} = \mu K \sum_s T_s \nabla \bar{n}_s$$

which can be simplified as

$$\nabla \left( \bar{\mathbf{B}}^2 / 2 + \mu K \sum_s T_s \bar{n}_s \right) = 0. \quad (2.8)$$

For a typical Harris current-sheet equilibrium, we choose the sheared and guiding magnetic field, and the equilibrium flow are transverse to the inhomogeneity, i.e.  $\bar{\mathbf{B}} = \hat{\mathbf{x}} \bar{B}_x(z) + \hat{\mathbf{y}} \bar{B}_y$ ,  $\bar{B}_x(z) = \bar{B}_{x0} \tanh(z/L)$ , and  $\bar{\mathbf{v}}_s = \hat{\mathbf{y}} \bar{v}_s$ , where

$$\begin{aligned} \bar{v}_s &= 2KT_s / (q_s \bar{B}_{x0} L), \quad \bar{n}_s(z) = n_{s0} n_s(z) = n_{s0} \text{sech}^2(z/L), \quad \text{for } s = he, hi, \\ \bar{v}_s &= 0, \quad n_s(z) = 1, \quad \text{for } s = be, bi \end{aligned}$$

which satisfy the equilibrium equations. Substituting the above quantities into Eq. (2.8) gives

$$\nabla \left( \left( \bar{B}_x^2/2 - \mu K \sum_{s=hi,he} T_s n_{s0} \right) \tanh^2(z/L) + \frac{\bar{B}_y^2}{2} + \mu K \sum_s T_s n_{s0} \right) = 0,$$

which holds the balancing between magnetic pressure and thermal pressure

$$\bar{B}_x^2/2 = \mu K \sum_{s=hi,he} T_s n_{s0}. \quad (2.9)$$

By linearizing the electron-static two-fluid equations (2.1-2.4), we obtain the first-order linear equations governing the perturbation

$$\begin{aligned} \partial_t \delta n_s + \nabla \cdot (\delta n_s \bar{\mathbf{v}}_s + \bar{n}_s \delta \mathbf{v}_s) &= 0, \\ m_s \bar{n}_s (\partial_t \delta \mathbf{v}_s + \bar{\mathbf{v}}_s \cdot \nabla \delta \mathbf{v}_s) &= q_s \bar{n}_s (\delta \mathbf{E} + \delta \mathbf{v}_s \times \bar{\mathbf{B}}) + q_s \delta n_s \bar{\mathbf{v}}_s \times \bar{\mathbf{B}} - K T_s \nabla \delta n_s, \\ \delta \mathbf{E} &= -\nabla \phi, \\ \epsilon \nabla^2 \phi &= -\sum_s q_s \delta n_s, \end{aligned}$$

which can be simplified by making use of the equilibrium profiles

$$(\partial_t + \bar{\mathbf{v}}_s \cdot \nabla) \delta n_s + \nabla \cdot (\bar{n}_s \delta \mathbf{v}_s) = 0, \quad (2.10)$$

$$m_s (\partial_t + \bar{\mathbf{v}}_s \cdot \nabla) \delta \mathbf{v}_s + m_s \Omega_s \bar{\mathbf{b}} \times \delta \mathbf{v}_s = -q_s \nabla \phi - K T_s \nabla (\delta n_s / \bar{n}_s), \quad (2.11)$$

$$\epsilon \nabla^2 \phi = -\sum_s q_s \delta n_s, \quad (2.12)$$

where  $\Omega_s = q_s B / m_s$  is the ion- or electron-gyrofrequencies, and  $\bar{\mathbf{b}} = \bar{\mathbf{B}} / \bar{B}$  is the parallel direction of magnetic field. Because the equilibrium is symmetric in  $x$  and  $y$  direction, we can assume that the spatial and time dependence of the small-amplitude perturbations is given by the eikonal form,  $\delta \phi = \bar{\phi}(z) \exp[i(k_x x + k_y y - \omega t)]$ , to allow drift modes propagating in a transverse plane to the direction of inhomogeneity. Then above Eqs. (2.10-2.12) go to

$$\begin{aligned} \omega_s \delta n_s + i \nabla \cdot (\bar{n}_s \delta \mathbf{v}_s) &= 0, \\ m_s \omega_s \delta \mathbf{v}_s + i m_s \Omega_s \bar{\mathbf{b}} \times \delta \mathbf{v}_s &= -i [q_s \nabla \phi + K T_s \nabla (\delta n_s / \bar{n}_s)], \\ \epsilon \nabla^2 \phi &= -\sum_s q_s \delta n_s, \end{aligned}$$

where  $\omega_s = \omega - \bar{v}_s k_y$  is Doppler shifted frequency, and operator  $\nabla = i \mathbf{k} + \hat{\mathbf{z}} \partial_z$ . A formal solution to the perturbed momentum equation is given by

$$\begin{aligned} \delta \mathbf{v}_s &= -i \omega_s \mathbf{u}_s / (q_s \bar{n}_s), \\ \mathbf{u}_s &= \chi_s \left[ \nabla \phi_s - i \Omega_s / \omega_s (\bar{\mathbf{b}} \times \nabla \phi_s) - (\Omega_s / \omega_s)^2 \bar{\mathbf{b}} \bar{\mathbf{b}} \cdot \nabla \phi_s \right], \\ \phi_s &= \epsilon (\phi + K T_s N_s / q_s), \\ N_s &= \delta n_s / \bar{n}_s, \end{aligned}$$

where  $\chi_s = \omega_{ps}^2 (\omega_s^2 - \Omega_s^2)^{-1}$ , and  $\omega_{ps}^2 = n_s q_s^2 / (\epsilon m_s)$  is ion or electron plasma frequency. Making use of the above results, one may eliminate perturbed velocity  $\delta v_s$  and obtains a set of wave functions which involves density perturbations and field perturbations only,

$$\begin{aligned}\bar{n}_s q_s N_s &= -\nabla \cdot \mathbf{u}_s, \\ \nabla^2 (\phi_s - \epsilon K T_s N_s / q_s) &= -\sum_s q_s \bar{n}_s N_s.\end{aligned}$$

Therefore, by introducing Debye length  $\lambda_{Ds}^2 = \epsilon K T_s / (n_{s0} q_s^2)$ , the above equations can be simplified to

$$\bar{n}_s q_s N_s = \left[ \chi_s \left( \mathbf{k}^2 - (\Omega_s / \omega_s)^2 (\bar{\mathbf{b}} \cdot \mathbf{k})^2 \right) - \partial_z (\chi_s \Omega_s / \omega_s \hat{\mathbf{z}} \cdot (\bar{\mathbf{b}} \times \mathbf{k})) \right] \phi_s - \partial_z (\chi_s \partial_z \phi_s), \quad (2.13)$$

$$(\partial_z^2 - \mathbf{k}^2) (\phi_s - \lambda_{Ds}^2 n_{s0} q_s N_s) = -\sum_s q_s \bar{n}_s N_s. \quad (2.14)$$

The thermal correction in the above equation (2.14) is ignorable for the long wavelength perturbations where  $k \lambda_{Ds} \ll 1$  and  $k_{\perp} \rho_e \ll 1$ . For the short-wavelength perturbations, the finite temperature effects could readily be incorporated with kinetic theory as shown by Yu Lin *et al.* [20], where electrons are gyrokinetic and ions fully kinetic. Therefore, in the long-wavelength regime, the resulting equations are

$$\begin{aligned}\rho_s n_s &= \left[ \chi_s \left( \mathbf{k}^2 - (\Omega_s / \omega_s)^2 (\bar{\mathbf{b}} \cdot \mathbf{k})^2 \right) - \partial_z (\chi_s \Omega_s / \omega_s \hat{\mathbf{z}} \cdot (\bar{\mathbf{b}} \times \mathbf{k})) \right] \phi - \partial_z (\chi_s \partial_z \phi), \\ (\partial_z^2 - \mathbf{k}^2) \phi &= -\sum_s \rho_s n_s,\end{aligned}$$

where  $\rho_s = n_{s0} q_s N_s$  is the normalized density perturbation. These two equations can be combined to a single one

$$\partial_z [(1 - \sum_s \chi_s) \partial_z \phi] - [\mathbf{k}^2 (1 - \sum_s \chi_s) + \sum_s \eta_s(z)] \phi = 0, \quad (2.15)$$

where the lower-hybrid oscillation,  $\omega_i^2 = \omega_{pi}^2 / (1 + \omega_{pe}^2 / \Omega_e^2)$ , will be revealed when the driving source  $\sum_s \eta_s$  goes to zero.  $\eta_s$  is defined as

$$\eta_s(z) = \chi_s (\Omega_s / \omega_s)^2 (\bar{\mathbf{b}} \cdot \mathbf{k})^2 + \partial_z [\chi_s \Omega_s / \omega_s \hat{\mathbf{z}} \cdot (\bar{\mathbf{b}} \times \mathbf{k})].$$

In the following part, we will concentrate in a case where the wave frequency  $\omega$  is much higher than the ion gyrofrequency, but much lower than the electron gyrofrequency defined with the asymptotic sheared field magnitude,  $B_{x0}$ , when  $z$  approaches to infinity,

$$\Omega_{i\infty} \ll \omega \ll |\Omega_{e\infty}|,$$

where  $\Omega_{i\infty} = e B_{x0} / m_i$  and  $\Omega_{e\infty} = -e B_{x0} / m_e$ . The characteristic frequency designates this frequency regime is the lower-hybrid frequency, which is defined as

$$\omega_{LH} \equiv \sqrt{\Omega_{i\infty} |\Omega_{e\infty}|} = e \bar{B}_{x0} / \sqrt{m_i m_e}.$$

In this frequency regime of interest, we may treat ions as if they are unmagnetized ( $\Omega_{i\infty} \sim 0$ ) while electrons as if fully magnetized. For the rest of this paper, we will work with the normalized variables:

$$\begin{aligned}\omega &= \tilde{\omega}\omega_{LH}, \quad \bar{v}_s = u_s V_A, \quad z = L\tilde{z}, \quad \mathbf{k} = \tilde{\mathbf{k}}\omega_{LH}/V_A, \quad q_s = e\tilde{q}_s, \quad \phi = KT_e\tilde{\phi}/e, \\ B &= \bar{B}_{x0}\tilde{B}(z), \quad \tilde{m}_s = m_s/\sqrt{m_i m_e}, \quad R = \omega_{phi0}^2/\omega_{LH}^2, \quad \tau = \frac{T_e}{T_i}, \quad \alpha = \frac{n_{bi}}{n_{hi}} = \frac{n_{be}}{n_{he}}, \\ M &= m_i/m_e, \quad S \equiv \text{sech}^2(z), \quad T \equiv \tanh(z), \quad kL = \tilde{k}\omega_{LH}L/V_A = \frac{\tilde{k}\sqrt{M}}{u_i(1+\tau)},\end{aligned}$$

where we define  $V_A = \bar{B}_{x0}/\sqrt{\mu n_{hi0} m_i}$  as the reference Alfvén speed. It is also assumed that  $\tilde{q}_s = \pm 1$  for simplicity, then we can get the following relations

$$\begin{aligned}\tilde{\omega}_{pbi0}^2 &= \alpha R, \quad \tilde{\omega}_{phe0}^2 = RM, \quad \tilde{\omega}_{pbe0}^2 = \alpha RM, \quad \tilde{\Omega}_{e0}^2 = M, \quad \tilde{\Omega}_{i0}^2 = 1/M, \\ \chi_{hi} &= \frac{RS}{\tilde{\omega}_{hi}^2 - \bar{B}^2/M}, \quad \chi_{bi} = \frac{\alpha R}{\tilde{\omega}^2 - \bar{B}^2/M}, \quad \chi_{he} = \frac{RMS}{\tilde{\omega}_{he}^2 - \bar{B}^2 M}, \quad \chi_{be} = \frac{\alpha RM}{\tilde{\omega}^2 - \bar{B}^2 M}, \\ \bar{u}_s &= \frac{1}{V_A} \frac{2KT_s}{q_s \bar{B}_{x0} L} \text{quad}(s=hi,he), \quad \frac{u_{he}}{u_{hi}} = -\tau, \\ \tilde{\omega}_{hi} &= \tilde{\omega} - \tilde{k}_y u_i, \quad \tilde{\omega}_{he} = \tilde{\omega} - \tilde{k}_y u_e = \omega + \tilde{k}_y \tau u_i.\end{aligned}$$

Therefore, the second order wave equation (2.15) becomes

$$\partial_z(A\partial_z\phi) + B\phi = 0, \quad (2.16)$$

where the coefficients are

$$\begin{aligned}A &= 1 - \frac{RS}{\tilde{\omega}_{hi}^2 - \bar{B}^2/M} - \frac{\alpha R}{\tilde{\omega}^2 - \bar{B}^2/M} - \frac{RMS}{\tilde{\omega}_{he}^2 - \bar{B}^2 M} - \frac{\alpha RM}{\tilde{\omega}^2 - \bar{B}^2 M}, \\ B &= \frac{M}{u_i^2(1+\tau)^2} \left[ (1 - \sum_s \chi_s) \tilde{\mathbf{k}}^2 + \sum_s \chi_s \left( \tilde{q}_s^2 \left( \frac{T\tilde{k}_x + \tilde{B}_y \tilde{k}_y}{\tilde{\omega}_s \tilde{m}_s} \right)^2 \right. \right. \\ &\quad \left. \left. + \frac{u_i(1+\tau)\tilde{q}_s}{\sqrt{M}\tilde{\omega}_s \tilde{m}_s} (S\tilde{k}_y + \partial_z \ln \chi_s (T\tilde{k}_y - \tilde{B}_y \tilde{k}_x)) \right) \right].\end{aligned}$$

These coefficients can be simpler by using  $m_i/m_e = \sqrt{|\Omega_e|/\Omega_i} \gg 1$

$$A = 1 - \frac{RS}{\tilde{\omega}_{hi}^2} - \frac{\alpha R}{\tilde{\omega}^2} + \frac{RS}{\bar{B}^2} + \frac{\alpha R}{\bar{B}^2},$$

$$B = \frac{M}{u_i^2(1+\tau)^2} \left[ (1 - \sum_s \chi_s) \tilde{\mathbf{k}}^2 + \chi_{he} \left( M \left( \frac{T\tilde{k}_x + \tilde{B}_y \tilde{k}_y}{\tilde{\omega}_{he}} \right)^2 - \frac{u_i(1+\tau)}{\tilde{\omega}_{he}} (S\tilde{k}_y + \partial_z \ln \chi_{he} (T\tilde{k}_y - \tilde{B}_y \tilde{k}_x)) \right) + \chi_{be} \left( M \left( \frac{T\tilde{k}_x + \tilde{B}_y \tilde{k}_y}{\tilde{\omega}} \right)^2 - \frac{u_i(1+\tau)}{\tilde{\omega}} (S\tilde{k}_y + \partial_z \ln \chi_{be} (T\tilde{k}_y - \tilde{B}_y \tilde{k}_x)) \right) \right].$$

## 2.1 Local limit

In the local limit, the spatial and time dependence of the small-amplitude perturbations is given by the eikonal form,  $\delta\varphi = \tilde{\varphi} \exp[i(k_y y + k_z z - \omega t)]$ , to allow drift modes propagating along and transverse to the direction of inhomogeneity  $z$ , and  $k_z L \gg 1$ . Then, wave equation (2.15) goes to

$$(k_z^2 + k_y^2) (1 - \sum_s \chi_s) + \sum_s \eta_s(z) = 0, \quad (2.17)$$

where the lower-hybrid oscillation,  $\omega_i^2 = \omega_{pi}^2 / (1 + \omega_{pe}^2 / \Omega_e^2)$ , will be revealed when the driving source  $\sum_s \eta_s$  goes to zero, and

$$\eta_s(z) = \partial_z [\chi_s \Omega_s / \omega_s \hat{\mathbf{z}} \cdot (\tilde{\mathbf{b}} \times \mathbf{k})].$$

## 3 Numerical analysis

A shooting code [19] has been developed to study the behavior of the eigenmodes, where the solution to the equations with boundary conditions at the two endpoints of an interval is found by launching "shots" from both sides of the interval and trying to match continuity conditions at an intermediate point. For the benchmark and verification purpose, the numerical solutions to Eq. (2.16) with guide field turned off has been obtained as a first step for a set of parameters

$$M = 1836, \quad R = 100, \quad \tau = 0.1, \quad u_{hi} = 1.$$

We turned off the background plasma,  $n_{bi}/n_{hi} = 0$ , and the guide field,  $B_y = 0$ . The solutions are computed at fixed wavelength along  $y$  axis,

$$\tilde{k}_y = ck_y / \omega_{pe} = 0.5,$$

which corresponds to  $k_y L \simeq 20$  in physical space. For these set of parameters, the ion gyroradius, electron gyroradius, ion sheath depth, and electron sheath depth are

$$\rho_i \sim 0.7L, \quad \rho_e = 0.005L, \quad d_i \equiv c / \omega_{pi} \sim 42.8L, \quad d_e \equiv c / \omega_{pe} \sim 0.02L.$$

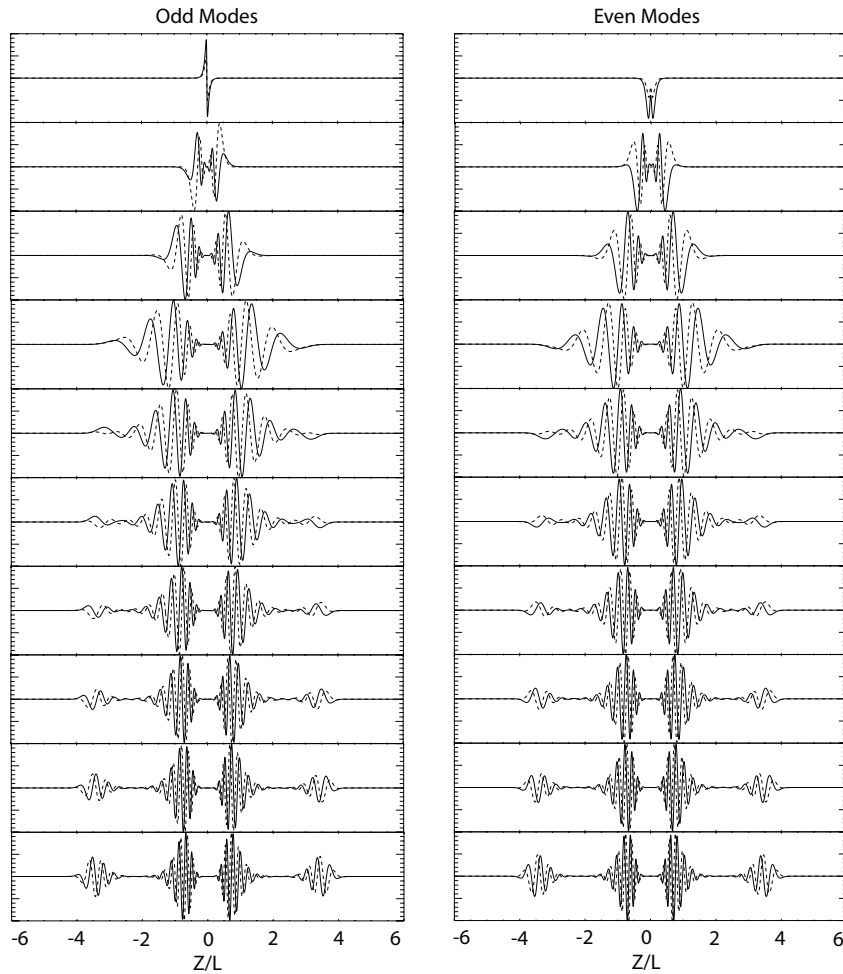


Figure 1: Mode structures associated with the lower-hybrid drift instabilities, where the electric potential  $\phi$  are plotted versus  $z/L$ , solid curves represent the real part of  $\phi$ , and the dotted curves stand for the imaginary part of  $\phi$ . Modes with node number 1,7,13, $\dots$ ,55 are selected as samples for odd-symmetrical eigenfunctions, and modes with node number 0,6,12, $\dots$ ,54 for even-symmetrical.

This suggests that the modes have much shorter wavelength than the current-sheet width, ion gyroradius, and ion sheath depth, but much longer than the electron gyroradius and sheath depth. On the other hand, this also confirms that 1) ions can be regarded as unmagnetized particles, and electrons as fully magnetized particles; 2) the assumption right after Eq. (2.14) is self-consistent for the current case.

In Fig. 1, some sample mode structures of eigenfunctions,  $\phi(z/L)$  versus  $z/L$ , has been shown in a stack format for two polarizations, even and odd, which corresponds to symmetry and antisymmetry structures, respectively:

$$\begin{aligned}\phi(-z/L) &= \phi(z/L), & \text{for even modes,} \\ \phi(-z/L) &= -\phi(z/L), & \text{for odd modes.}\end{aligned}$$

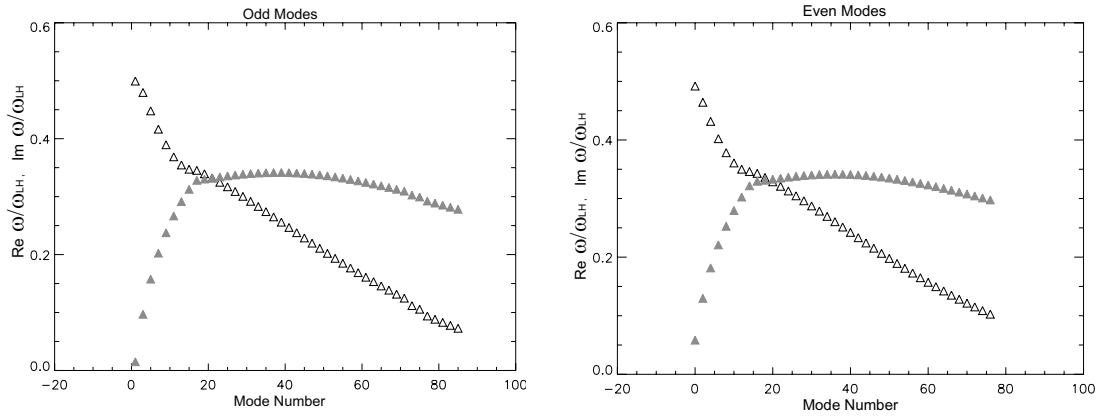


Figure 2: Real ( $\Delta$ ) and imaginary ( $\blacktriangle$ ) parts of the eigenvalues,  $\text{Re}\omega/\omega_{LH}$  and  $\text{Im}\omega/\omega_{LH}$ , corresponding to the solutions shown in Fig. 2, versus the mode number:  $1,3,5,\dots$ , for odd modes, and  $0,2,4,\dots$ , for even modes.

Each mode has been designated by a quantum-like mode number,  $1,3,5,\dots$ , for odd modes, and  $0,2,4,\dots$ , for even symmetries according to their node numbers, which is defined as the number of zeros on the  $z/L$  axis. It shows that there are multiple eigenstates for both symmetries, reminiscent of the multilevel eigenvalue problem of quantum mechanics. The eigenfunctions situated closest to the neutral sheet,  $z/L=0$ , can be identified as the ground-state solutions. As the mode number increases, it can be seen that the degree of undulations associated with  $\phi$  increases, and the wave packet keeps moving away from the neutral sheet, at the same time, the characteristic length of the wave packet shrinks gradually from about  $L/2$  to  $L/16$ . For large number modes, the wave reaches its extremum around the edge of the current sheet,  $z \simeq L$ , where the density gradient gets its maximum.

The eigenvalues,  $\omega/\omega_{LH}$ , corresponding to the solutions shown in Fig. 1 are displayed in Fig. 2 as a function of the mode number. For both symmetries, the real frequency,  $\text{Re}\omega/\omega_{LH}$ , ranges from  $0.5\omega_{LH}$  to  $0.1\omega_{LH}$ , locates in the lower-hybrid regime, and decreases as the mode number increases. The behavior of the growth rate,  $\text{Im}\omega/\omega_{LH}$ , versus mode number is of great interest. It can be seen that the ground state modes for either symmetry, which situated at the current sheet center, have the lowest growth rate, which are long-wavelength perturbations. The growth rate sharply increases with the mode number for low modes, then goes to the fast growing region and gains its maximum when the mode number is around 40. These most unstable modes are lower-hybrid short-wavelength perturbations.

## 4 Conclusions and discussions

In the current paper, we have constructed a nonlocal electrostatic two-fluid model for the lower-hybrid drift instabilities with a guide field. A wave equation for LHDI has

been obtained. Numerical solution to the wave function has been carried out with guide magnetic field turned off for benchmarking and validation purpose.

It is found out that for either symmetries, odd and even, there are multiple eigenstates, which are designated by a mode number according to their node numbers. The ground state with the smallest mode number locates at the center of the current sheet and has the lowest growth rate. As the mode number increases, the wave packet moves away from the neutral sheet. The most unstable modes appear in high-mode region.

The present work is only a part of the first steps to investigate the fast reconnection mechanism, and eventually the gyrokinetic simulation of fast reconnection will be carried out with finite guide field. Comparisons with kinetic theory will be made in the near future in order to examine the validity of the fluid theory.

## Acknowledgments

The authors acknowledge fruitful discussions with Liu Chen, and Yu Lin. This work was supported by Department of Energy (DOE) Grants No. DE-FG02-07ER54916 (UC Irvine) and DE-FG02-05ER54826 (Auburn University), NSF Grant No. ATM-0449606, and Los Alamos National Laboratory Subcontract No. 50219-001-07.

## References

- [1] D. Biskamp, *Magnetic Reconnection in Plasmas*, Cambridge University Press, Cambridge, England, 2000.
- [2] P. Sweet, in: B. Lehnert (Ed.), *Electromagnetic Phenomena in Cosmical Physics*, Cambridge University Press, New York, 1958, pp. 123.
- [3] E. Parker, *J. Geophys. Res.* 62 (1957) 509.
- [4] H. Petschek, *NASA Spec. Publ.* 50 (1964) 425.
- [5] D. Biskamp, *Phys. Fluids* 29 (1986) 1520.
- [6] R. Kulsrud, *Earth Planets Space* 53 (2001) 417.
- [7] T. Carter, H. Ji, F. Trintchouk, M. Yamada, R. Kulsrud, *Phys. Rev. Lett.* 88 (2002) 015001-1.
- [8] D. B. Batchelor, R. C. Davidson, *Phys. Fluids* 19 (1976) 882.
- [9] R. C. Davidson, *Phys. Fluids* 19 (1976) 1189.
- [10] G. Ganguli, Y. C. Lee, *Phys. Fluids* 31 (1988) 823.
- [11] G. Ganguli, Y. C. Lee, *Phys. Fluids* 31 (1988) 2753.
- [12] H. Romero, G. Ganguli, Y. C. Lee, *Phys. Fluids B* 4 (1992) 1708.
- [13] N. T. Gladd, S. H. Brecht, *Phys. Fluids B* 3 (1991) 3232.
- [14] A. T. Y. Lui, C.-L. Chang, P. H. Yoon, *J. Geophys. Res.* 100 (1995) 19147.
- [15] P. H. Yoon, A. T. Y. Lui, *J. Geophys. Res.* 101 (1996) 4899.
- [16] P. H. Yoon, A. T. Y. Lui, *J. Geophys. Res.* 106 (2001) 13203.
- [17] J. D. Huba, J. F. Drake, N. T. Gladd, *Phys. Fluids* 23 (1980) 552.
- [18] P. H. Yoon, A. T. Lui, M. I. Sitnov, *Phys. Plasmas* 9 (2002) 1526.
- [19] W. H. Press, S. A. Teukolsky, W. T. Vetterling, B. P. Flannery, *Numerical Recipes in FORTRAN* 77, Cambridge University Press, Cambridge, England, 1995.
- [20] Y. Lin, X. Wang, Z. Lin, L. Chen, *Plasma Phys. Controlled Fusion* 47 (2005) 657.
- [21] W. Daughton, *Phys. Plasmas* 10 (2003) 3103.